American Mineralogist, Volume 60, pages 998–1012, 1975

Studies of the Sulfosalts of Copper. IV. Structure and Twinning of Sinnerite, $Cu_6As_4S_9$

EMIL MAKOVICKY

Mineralogical Institute, University of Copenhagen, Copenhagen K, Denmark

AND BRIAN J. SKINNER

Department of Geology and Geophysics, Yale University, New Haven, Connecticut 06520

Abstract

Sinnerite, $Cu_6As_4S_9$, is triclinic, $a = 9.064$ Å, $b = 9.830$ Å, $c = 9.078$ Å, $\alpha = 90°00'$, $\beta = 109°30'$, $\gamma = 107°48'$, $Z = 2$, and space group $P\bar{1}$. The structure is based on a sphalerite-like substructure and contains two kinds of twisted, chain-like groups of $[AsS_3]$ pyramids; one group contains 3 pyramids, the other 5 pyramids. Every S atom in the structure belongs to one of the groups and is bound to one or two As atoms, leading to the structural formula $Cu_{12}[As_3S_7][As_5S_{11}]$. The structure of sinnerite may be viewed as a close packing of the two groups stacked parallel to [001]. Each kind of group forms indistinct layers parallel to (010). Disorder in the packing sequences of the two groups, due to their internal symmetry and configurational similarities, leads to the twin laws $n\|(1\bar{1}0)$, $n\|(010)$, $m\|(\bar{4}14)$, and $2\|[101]$. Four As atoms, each belonging to a distinct group, occur around each of the two vacant S positions per unit cell, giving mutually interconnected $[As_4S_{12}]$ clusters of $[AsS_3]$ pyramids. All Cu atoms are tetrahedrally coordinated. The twinning produces twin aggregates which contain 24 individuals and simulate $\bar{4}3m$ cubic symmetry.

Introduction

The sulfosalts of copper are a compositionally diverse and structurally complex group of minerals. The most abundant members of the group are the isostructural compounds tennantite and tetrahedrite, which have structures derived from sphalerite (Wuensch, Takeuchi, and Nowacki, 1966). Three other copper sulfosalts—nowackiite, sinnerite, and "phase A", a synthetic compound described by Maske and Skinner (1971)—also have structures derived from sphalerite. Neither nowackiite nor sinnerite are known to be common minerals, but the possibility that either or both may indeed be widespread should not be overlooked, because both resemble tennantite and tetrahedrite, and both may commonly have been mistaken for them in natural assemblages.

Sinnerite, the subject of this paper, has been described from only a single locality—the Lengenbach Quarry, Binnenthal, Switzerland (Marumo and Nowacki, 1964). Its composition and symmetry were determined by Makovicky and Skinner (1972) from material synthesized by Maske and Skinner (1971) during their study of the system Cu–As–S. Its composition, $Cu_6As_4S_9$, corresponds to $3Cu_2S + 2As_2S_3$, which makes it the most As-rich ternary compound on the pseudobinary join Cu_2S–As_2S_3. The symmetry is triclinic and the dimensions of the primitive unit cell are $a = 9.064 \pm 0.008$ Å, $b = 9.830 \pm 0.008$ Å, $c = 9.078 \pm 0.008$ Å, $\alpha = 90°00' \pm 20'$, $\beta = 109°30' \pm 20'$, and $\gamma = 107°48' \pm 20'$. Each unit cell contains two formula units of $Cu_6As_4S_9$.

The sphalerite-like substructure of sinnerite, which is only slightly deformed from ideal cubic symmetry, gives rise to an extremely pronounced subcell with dimensions $a = 5.25$ Å, $b = 5.25$ Å, $c = 5.23$ Å, $\alpha = 89°59'$, $\beta = 89°52'$ and $\gamma = 90°14'$. The subcell is related to the true cell of sinnerite by the matrix

−0.1	+0.4	+0.3
−0.4	−0.4	+0.2
+0.5	0.0	+0.5

Both natural and synthetic crystals of sinnerite are complexly twinned. Makovicky and Skinner (1972) demonstrated that, within the synthetic crystals

studied, twinning occurred by reticular pseudomerohedry.

Measurement Procedure

Crystals of sinnerite suitable for crystal-structure analysis were prepared at 450°C, by reaction of spectrographically pure elements in evacuated silica vessels. Because all crystals produced were twinned, it was necessary to select a needle-shaped twin aggregate with which to work. The twin aggregate chosen has dimensions $0.07 \times 0.05 \times 0.2$ mm, but is favorable for X-ray studies because only two twin orientations—those related by the twin plane (010)—are prominent. Each orientation is present in approximately equal volumes. The remaining four twin orientations are also present, but only in very minor amounts. X-ray diffraction intensities were measured in Mo$K\alpha$ radiation using an ω-2θ scan on the Picker PT, four-circle diffractometer of the U. S. Geological Survey in Washington, D. C. Intensities were corrected for background, and for Lorentz and polarization effects. From the 2800 independent reflection positions measured, only about 900 reflections were strong enough to be detected. From this set of 900, approximately 200 mutually overlapping reflections were discarded. Discarded reflections were (1) all true-cell reflections with $h = 4n + l$ (due to twin law (010); (2) all reflections with $k + h = 5n - 2l$ (due to twin law (T10); and (3) all subcell reflections (due to overlap by all twin laws). In addition, certain reflections were removed because of large fluctuations in background intensities. Such fluctuations were taken to indicate accidental or incomplete overlap of some reciprocal lattice spots with indices that do not obey the previous criteria.

Absorption corrections were applied to each of the accepted reflections by approximating the crystal to a flattened eight-sided prism and using a program written by C. T. Prewitt after the method of Wuensch and Prewitt (1965). A grid of $12 \times 12 \times 12$ diffraction points was employed, and weights were assigned to each point in order to simulate the equal-volume polysynthetic twinning as determined by optical examination of polished surfaces of sinnerite. Due to the small size and the complex morphology of the crystal used, the true distribution of the two main twin components in it could not be established.

Unfortunately most true-cell reflections of sinnerite are close to the limits of detection. Consequently, the intensity-to-background ratio is low and the resulting measurement accuracy poor. For the strongest reflections σ_F represents about 4 percent of the F value, but for the majority of detectable reflections σ_F values range from 10 to 20 percent of the respective F values.

Determination of Crystal Structure

Prediction

Physical properties and chemical composition indicate that sinnerite possesses a defective sphalerite-type structure and that two sulfur sites in each unit cell are vacant. The sphalerite-type substructure permits only one space group—the acentric group $P\bar{1}$.

The low intensity ratios observed for reflections from the true cell, compared to those from the subcell, mean that such deviations from the ideal substructure as do occur must be very small. If there were no positional deviations from the ideal substructure sites, an average metal site would be occupied by 2/5 As + 3/5 Cu atoms, yielding 30.6 electrons. Similarly, an average sulfur site would be occupied by 9/10 S atoms, yielding 14.4 electrons. In a Fourier "map" calculated solely on the basis of true-cell reflections, then, As atoms will be characterized by an excess of 2.4 electrons per atom, while Cu atoms will be characterized by a deficiency of 1.6 electrons, and S atoms by an excess of 1.6 electrons. Vacant sulfur sites, henceforward designated S_v, will be characterized by a deficiency of 14.4 electrons per site. Due to position shifts away from the substructure, however, average atomic sites will become broadened, so that considerably lower peak electron densities should be observed. Therefore, electron density differences produced by As and S atoms situated close to the average atomic sites will be heightened, while the negative values predicted for Cu may reach zero, or even become positive. Vacant sites and atoms with large deviations from average sites will contribute more strongly to the true-cell reflections than do atoms in or close to average sites.

From the composition of sinnerite, we can anticipate that it contains trivalent As atoms coordinated to three S atoms in a trigonal-pyramidal array. The $[AsS_3]$ pyramids can replace some of the $[MeS_4]$ tetrahedra in the sphalerite-type substructure. Because the S–As–S angles at the apices of the trigonal pyramids are smaller than the S–Me–S angles in the tetrahedra (Takeuchi and Sadanaga, 1969), As atoms can be expected to display the largest deviations from the average atomic sites. An As atom should therefore create a strong maximum in the Fourier "map", and with it should be a smaller minimum corresponding to the vacant average site.

From the behavior observed in tennanite (Wuensch *et al,* 1966), and in nowackiite (Marumo, 1967), we can predict that deviations of As atoms away from the center of the tetrahedron will be toward the vacant S position. A Patterson function of the tetrahedral structure of sinnerite will have all Me–Me and S–S vectors concentrated in the tetrahedral apices, while the Me–S vectors will be directed towards the centers of the tetrahedra. Therefore, we can anticipate that the S_v–S_v vectors with their positive maxima will be obscured by the clusters of overlapping maxima and minima from the overlapping Me–Me vectors. The As–S_v vectors, however, should be the most prominent of all the Me–S vectors in the Patterson function; there should be 8 As–S_v vectors for each vacancy, and each should give rise to a minimum.

Observed

The actual 3-dimensional Patterson function of sinnerite shows that one set of the probable As–S_v vectors—those parallel to the *c* axis—are especially prominent (Fig. 1). These As–S_v pairs, which are related to each other by the vector (0.36, 0.60, 0.46),

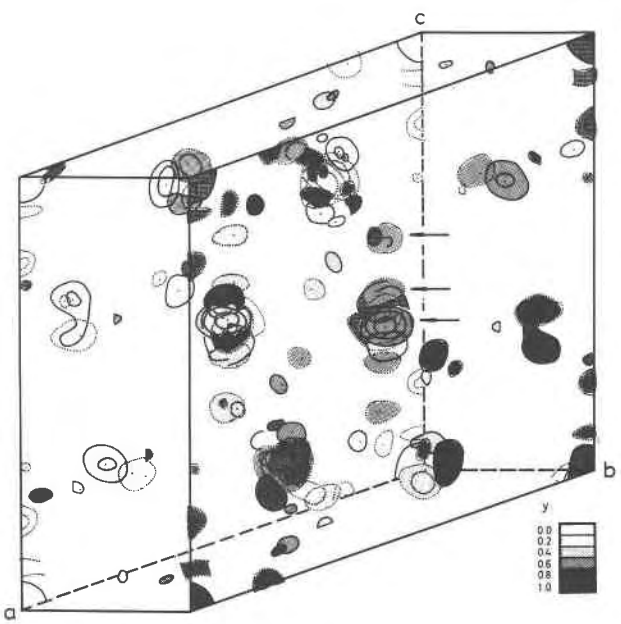

FIG. 1. Three-dimensional Patterson function of sinnerite (true-cell reflections only). Projection on (010), with clustering of maxima and minima in the vertices and centers of the tetrahedral motive. Equal arbitrary increments of the difference in true-cell and subcell squared electron densites (except at the origin). Positive maxima given in full, negative in dotted outlines. Arrows indicate the features created by the outstanding vertical As–S_v pairs.

were therefore used as the starting set of atoms for the first structure factor calculations, which yield an initial *R* value of 46 percent.

The first Fourier "maps" revealed the "heavy-atom" character of the difference structure. It was therefore decided to carry out first the structure determination on a difference level. The two negative sulfur vacancies and the positive maxima observed in the Fourier "maps" were substituted successively by appropriate atoms, then the site occupancy refined on the difference level. Although the low number of structure factors available led to confusing false maxima, this approach revealed all the basic contributors to the true-cell reflections. The basic contributors are, first, the S_v sites; second, most of the As atoms around the S_v sites; and third, the three Cu atoms arranged in a spiral parallel to the *c* axis. Identity of atomic configurations around the two vacancies, which was revealed in later stages of the structure determination, complicated the solution by representing an overlap of two identical structures mutually displaced by the S_v–S_v vector. The difference structure was brought to an *R* value of 15 percent, but, even so, some Cu and S atoms did not become clearly visible above background.

The difference structure was raised to a full site occupancy situation by substituting Me and S atoms for the observed maxima, and by introducing them into the remaining unresolved average positions. The subsequent refinement attempts were performed with the full-matrix, least squares program, ORFLS (Busing, Martin, and Levy, 1962), to which full-scale, acentric, anomalous dispersion corrections had been added by one of us (E.M.). For the three-dimensional Fourier synthesis, the program NRC-8 (Ahmed, 1968) was employed. Scattering form factors for non-ionized Cu, As, and S atoms, and anomalous dispersion coefficients, were taken from Cromer and Waber (1965) and Cromer (1965) respectively. The approximate character of the absorption correction made it necessary to introduce a separate scale factor for each reciprocal lattice level along the needle (*c*) axis. Because of the small number of reflections available, only an overall temperature factor was normally employed. All atomic sites were assigned unit occupancies.

There are 38 independent atoms in the unit cell of sinnerite. This means there are either 5 or 6 observed reflections per positional parameter, considerably fewer than employed in structure determination of similar compounds (Wuensch *et al,* 1966; Marumo, 1967). Therefore, all features specific to the difference

structure determination became an important limiting factor in the refinement. Both site occupancies and individual temperature factors correlate strongly with positional parameters. Atoms can be moved along the boundary between their substructure maximum and the related minimum (Fig. 2) with only small effects on the R value; the positional parameters involved are strongly correlated. The (F_o-F_c) values of the difference structure, however, are sensitive to small positional shifts directed across these boundaries and the steep and high R-value barriers around the correct sites may result in convergences on local false minima.

Several separate attempts were made to populate the indistinct atomic positions of the difference structure, using structure factors with assigned unit weights. The best results were then used for further refinement attempts using weighted structure factors. Experimental errors of the structure factors have substantial influence on the quality of refinement in the case of sinnerite, and by introducing weights equal to $1/\sigma_F$ a substantial improvement of atomic positions was achieved. Both of the centrosymmetrically related orientations of the structure were then refined using anomalous dispersion coefficients, and the orientation with the lower R value was then chosen.

The refinement using 607 measured intensities was stopped at an R_{weighted} value of 15.8 percent ($R_{\text{unweighted}}$ = 17.2%), when positional changes had reached values far below their standard deviations (Table 1). Its results were then used for a final refinement attempt employing 170 additional, randomly chosen undetectably weak reflections, for which F_o values were derived, using the detectability threshold of the measuring device and the same corrections as used for the measured reflections. Structure factors were again assigned unit weights in order to stress the role of the undetected reflections, and the refinement carried out to an R value of 22.7 percent, when it was terminated due to slow convergence. In spite of the problematic quality of the undetected reflections in the reciprocal space containing six lattices, their addition to the refinement did produce a marked improvement in several of the "heavy-atom" positions and in the z co-ordinates of the sulfur atoms (Table 2).

Description of Crystal Structure

As described in the previous section, experimental and correlation-produced errors limited the accuracy of the structure refinement, especially on the sulfur positions. The highest correlation coefficients have values of about 0.6. The average trigonal-pyramidal As–S and the average tetrahedral Cu–S bond lengths are 2.27 and 2.29 Å compared to the expected values of 2.25 Å and 2.33 Å, respectively. The standard error, however, exceeds 0.30 Å so that no precise coordination properties of the elements involved can be described. The coordination polyhedra of Cu and As^{III} differ from each other in all known structures both in the number and the coordination of the atoms involved. This fact, together with the ratios of Fourier maxima to the related minima, enabled an unambiguous distinction between copper and arsenic in the metal positions. Thus, we were able to decipher all the principal features of the crystal structure of sinnerite, including the size, shape, and packing scheme of different [As_iS_j] groups. The order-disorder (OD) phenomena, derived from the established packing scheme, explained completely the observed twinning laws. Further refinement of the structure of this strongly X-ray absorbing mineral will only be achieved if a sufficiently large untwinned crystal is found. Both the OD nature of twinning and the practical experience on synthetic and natural material indicate that the chances of such a find are extremely small.

The crystal structure of sinnerite is based on a sphalerite-like substructure with 8 out of 20 tetrahedra per triclinic unit cell replaced by trigonal [AsS_3] pyramids. These are clustered in two groups, four pyramids in each, to give [As_4S_{12}] clusters

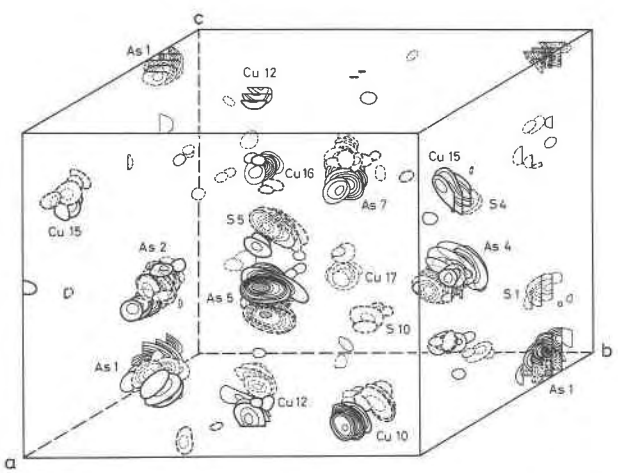

FIG. 2. Part of the three-dimensional Fourier function of sinnerite (true-cell reflections only; consecutive sections spaced by 1/40 of a). Maxima (full outlines) and minima (broken outlines) shown between x = 17/40 (front face) and x = 2/40. Equal arbitrary increments of the difference electron density, with extreme values shaded. Three grades of outline boldness indicate the approximate x coordinate of the sections.

around the two vacant S positions of each unit cell. Such a cluster, together with its schematic representation, is depicted in the lower-most portion of Figure 8. The As atoms are displaced towards the vacant site at the center of each cluster, so that the As–As distances, which average 3.3 Å, are close to the van der Waals As–As distances of 3.15 Å between adjacent layers of pure arsenic (Bradley, 1924).

TABLE 1. Observed and Calculated Structure Factors for Sinnerite

h	k	l	F_o	F_c	h	k	l	F_o	F_c	h	k	l	F_o	F_c	h	k	l	F_o	F_c	h	k	l	F_o	F_c	h	k	l	F_o	F_c
-3	0	0	22.1	22.4	0	-5	1	22.6	24.9	-8	-5	2	22.0	24.0	-3	6	3	16.9	18.6	-5	1	5	26.3	30.7	-4	9	6	17.5	21.1
-3	0	0	18.1	21.0	2	-5	1	14.1	21.7	-1	6	2	23.3	17.4	-3	-6	3	14.9	12.9	-5	-1	5	10.6	16.3	-4	-9	6	16.6	24.6
6	0	0	14.7	11.7	-4	5	1	14.3	10.4	1	-6	2	15.7	16.4	6	-6	3	37.4	28.8	6	1	5	20.6	15.3	-8	9	6	19.6	16.1
2	1	0	14.2	10.4	-4	-5	1	27.2	33.6	-3	6	2	18.0	21.5	-6	-6	3	28.0	20.3	7	-1	5	13.5	20.9	0	0	7	16.7	19.4
-2	1	0	10.3	5.7	-5	5	1	11.2	9.8	-4	6	2	31.9	30.1	-8	6	3	15.2	19.6	0	-2	5	19.1	19.4	2	0	7	29.9	27.1
2	-1	0	13.5	7.2	7	-5	1	20.5	20.9	-7	6	2	20.0	18.2	9	-6	3	24.9	21.1	-1	2	5	33.7	29.7	-3	0	7	30.5	40.1
5	1	0	11.1	15.9	-8	5	1	23.4	21.8	-8	6	2	14.8	17.8	-11	6	3	15.6	23.0	3	-2	5	23.8	21.6	-6	0	7	14.7	23.4
-5	1	0	11.7	8.4	-9	5	1	17.9	16.7						2	-7	3	42.2	44.4	-4	2	5	16.2	21.0	1	-1	7	15.4	17.0
-5	-1	0	13.8	16.5	0	-6	1	29.2	26.5	8	-6	2	24.6	15.9	-3	-7	3	18.9	13.9	-4	-2	5	13.8	17.3	-2	1	7	44.6	41.3
-7	1	0	11.7	13.3	-2	6	1	29.2	31.6	0	7	2	15.5	9.9	4	7	3	28.8	28.2	-6	-2	5	12.5	15.9	-2	-1	7	49.9	48.2
7	-1	0	12.5	14.1	2	-6	1	17.5	17.3	1	7	2	19.4	17.6	-4	7	3	16.6	19.1	0	3	5	31.3	32.2	-3	1	7	12.7	17.9
-7	-1	0	19.1	23.1	-4	6	1	24.5	25.1	1	-7	2	19.2	27.9	-7	7	3	35.0	36.3	-1	3	5	15.9	13.6	-4	1	7	14.4	13.2
1	2	0	12.0	16.1	-4	-6	1	17.2	15.8	-3	7	2	23.3	35.1	0	8	3	17.4	23.7	-1	-3	5	22.1	23.2	4	-1	7	14.9	16.1
1	-2	0	9.3	6.7	-5	6	1	14.0	15.6	-3	-7	2	25.9	28.6	-2	8	3	20.1	14.0	-2	3	5	35.3	28.6	-4	-1	7	26.5	25.0
-3	2	0	11.9	17.5	6	-6	1	14.9	6.7	-7	7	2	12.7	8.7	-3	8	3	30.1	31.0	2	-3	5	12.1	19.6	-7	1	7	14.8	11.4
-5	-2	0	17.9	22.6	-9	6	1	11.9	10.4	7	-7	2	24.0	20.9	-4	-8	3	19.7	22.7	3	3	5	20.4	24.7	-7	-1	7	30.0	32.7
-6	2	0	15.9	19.2	0	7	1	21.4	34.2	-8	7	2	14.0	18.4	-2	9	3	34.9	34.3	-4	3	5	21.0	11.3	0	-2	7	23.1	25.3
8	-2	0	11.6	19.7	2	7	1	31.4	38.0	9	-7	2	23.6	19.7	-4	9	3	15.6	15.6	4	-3	5	25.0	27.1	2	2	7	39.0	35.0
-1	3	0	16.5	12.7	2	-7	1	19.2	15.6	-1	8	2	31.2	32.8	-6	9	3	16.1	19.7	-5	3	5	11.1	16.7	-2	2	7	21.8	23.4
-2	3	0	11.5	12.5	-2	-7	1	16.0	16.4	1	-8	2	12.3	21.4	6	-9	3	14.9	7.8	-5	-3	5	14.3	13.3	-3	2	7	21.3	20.6
2	-3	0	12.9	11.7	4	-7	1	12.9	20.3	3	-8	2	34.3	41.9	-7	9	3	14.9	21.2	-6	3	5	12.1	8.1	-4	2	7	24.1	23.9
5	3	0	14.5	14.0	7	-7	1	14.6	21.9	-3	-8	2	34.8	35.4						0	-4	5	37.8	32.4	6	-2	7	19.3	24.1
-5	3	0	12.6	6.5	-8	7	1	18.2	14.7	-4	8	2	19.5	19.6	0	10	3	19.5	12.6	-1	4	5	20.6	19.9	-6	-2	7	30.9	40.0
1	-4	0	16.9	19.3	8	-7	1	17.2	13.2	5	-8	2	30.6	26.8	-4	10	3	23.9	29.2	2	4	5	21.7	25.2	-8	-2	7	25.6	22.5
-2	4	0	9.2	7.6	0	-8	1	30.3	27.4	0	9	2	15.9	18.4	5	-10	3	17.1	22.0	-2	5	5	24.5	20.9					
-2	-4	0	10.8	8.9	2	-8	1	17.0	23.8	-1	9	2	38.3	37.8	1	-11	3	17.8	12.6	-2	-4	5	17.8	18.9	0	3	7	27.2	24.3
-3	4	0	16.3	16.6	-4	8	1	30.9	25.2	1	-9	2	31.1	35.3	6	-11	3	18.3	17.7	3	4	5	14.6	11.6	0	-3	7	14.0	10.9
3	-4	0	17.2	17.1	4	-8	1	14.5	14.9	3	-9	2	18.5	10.0	1	0	4	14.2	20.5	-4	-4	5	16.9	19.3	2	-3	7	30.3	34.9
-5	4	0	24.5	21.2	-6	9	1	12.8	19.1	4	-9	2	22.2	21.6	-2	0	4	31.2	37.0	-5	4	5	11.4	14.9	-4	-3	7	24.9	20.4
5	-4	0	23.1	22.4	-9	8	1	22.6	20.9	-3	10	2	45.2	36.5	3	0	4	25.4	26.1	-5	-4	5	19.9	22.1	-6	3	7	21.4	20.2
-5	-4	0	17.2	13.7	0	-9	1	31.6	30.5	-7	10	2	24.1	30.6	-6	0	4	12.6	14.2	2	5	5	22.8	22.5	-8	3	7	28.4	26.9
-6	4	0	14.2	17.1	-4	9	1	24.5	20.5	-8	10	2	20.4	25.4	-1	1	4	41.8	36.2	3	5	5	20.7	20.9	-2	-4	7	35.5	26.8
-7	4	0	17.8	13.6	4	-9	1	13.4	20.1	1	-11	2	23.0	18.9	-1	-1	4	43.2	43.0	4	-5	5	12.7	13.4	-4	4	7	20.8	20.5
7	-4	0	16.0	15.0	2	-10	1	36.5	30.8	-3	11	2	18.1	15.2	2	1	4	26.1	32.5						6	-4	7	21.4	24.4
10	-4	0	17.5	10.1	2	-11	1	29.3	22.2	-4	11	2	15.2	16.5	-2	1	4	15.6	12.2	-4	-5	5	21.3	29.8	-7	4	7	48.0	47.9
1	5	0	25.2	27.5	-2	11	1	26.3	29.3	4	-11	2	12.5	14.1	2	-1	4	16.3	18.1	-6	5	5	15.6	15.6	0	-5	7	18.9	20.2
-1	-5	0	28.6	25.8	3	-12	1	24.4	16.2	1	-12	2	31.6	23.5	-3	1	4	16.0	20.1	-9	5	5	24.8	26.8	2	-5	7	41.3	46.0
1	-5	0	30.2	25.8	0	0	2	10.2	14.7	-3	12	2	32.8	26.4	-3	-1	4	26.2	25.8	4	-6	5	20.3	20.4	-3	5	7	38.7	41.6
-1	-5	0	23.1	28.1	3	0	2	26.0	28.4	1	0	3	14.9	8.0	-5	1	4	13.2	17.2	-5	6	5	24.6	27.7	-3	-5	7	29.2	22.3
-3	5	0	17.5	15.5	-3	0	2	14.8	21.7	2	0	3	34.2	36.1	5	-1	4	14.0	13.9	7	-6	5	18.2	10.9	-6	5	7	23.6	30.8
3	-5	0	11.8	14.1	-5	0	2	15.2	15.5	-3	0	3	13.7	16.4	-6	-1	4	23.9	26.2	-8	6	5	12.2	17.6	-7	5	7	14.5	17.1
-3	-6	0	23.0	23.2	7	0	2	16.4	7.2	-4	0	3	15.4	15.3	-7	1	4	18.9	14.9	0	-7	5	12.8	11.7	-2	6	7	41.6	37.3
3	-6	0	15.9	12.9	-8	0	2	31.2	32.4	-7	0	3	19.5	15.1	1	2	4	21.5	16.0	-1	7	5	28.3	23.4	-2	-6	7	55.6	57.5
-7	-6	0	20.2	26.0	1	1	2	10.1	16.0	-10	0	3	13.9	9.0	-1	2	4	24.8	23.8	-4	7	5	21.3	28.8	-3	6	7	21.7	18.4
11	7	0	20.7	17.8	-1	1	2	16.4	9.5	0	1	3	31.1	33.0	1	-2	4	14.8	18.6	-4	-7	5	19.0	25.4	-4	-6	7	24.4	20.5
1	-7	0	17.9	16.9	1	-1	2	10.2	6.1	1	1	3	11.0	23.1	2	2	4	16.3	5.6	-5	7	5	12.8	15.9	-7	6	7	17.5	18.5
-6	-7	0	16.1	15.1	-1	-1	2	16.9	9.4	1	-1	3	21.9	24.0	-2	-2	4	14.2	19.1	-8	7	5	12.7	17.8	-8	6	7	18.3	18.6
1	-8	0	19.5	22.6	3	-1	2	14.5	18.1	-2	-1	3	19.3	21.1	2	-2	4	15.2	19.9	-9	7	5	21.4	14.6	-3	7	7	24.8	21.4
2	-8	0	15.8	7.8	4	1	2	21.1	14.1	-3	1	3	22.4	24.0	-2	-2	4	25.9	19.9	0	-8	5	16.0	19.5	-4	7	7	23.4	22.0
-7	8	0	18.1	18.0	-4	1	2	34.0	32.0	-3	-1	3	19.3	18.4	3	2	4	33.3	34.8	-2	8	5	38.6	33.1	0	8	7	25.4	20.2
-10	9	0	15.0	15.2	4	-1	2	12.1	13.5	4	1	3	11.0	15.4	-3	2	4	21.9	21.3	-4	8	5	21.3	19.6	-2	-8	7	20.8	19.2
										-4	1	3	13.5	9.8	5	-2	4	11.1	22.8	4	-8	5	17.3	23.8	-4	9	7	18.4	24.0
3	0	1	15.3	21.9	-4	-1	2	17.2	24.9	5	1	3	19.3	6.8	-5	-2	4	25.3	29.3	0	-9	5	22.4	25.4	1	0	8	12.8	12.1
-3	0	1	27.7	26.8	7	1	2	27.3	22.7	6	1	3	28.1	23.8	-6	2	4	12.7	14.8	-2	9	5	23.4	24.1	-2	0	8	20.0	14.7
3	-2	1	24.1	28.1	-7	1	2	18.5	11.6	-6	1	3	18.8	10.2	-7	-2	4	14.0	17.7	3	-10	5	15.7	17.1	-5	0	8	30.3	30.2
-4	-3	1	13.2	20.5	-7	-1	2	17.7	13.6	-6	1	3	18.0	21.0	1	-3	4	15.7	11.7	0	0	6	16.5	16.8	-1	1	8	34.9	33.9
5	-3	1	24.2	26.7	-8	1	2	14.7	16.3	-7	-1	3	12.2	17.1	-2	3	4	10.8	14.6	1	0	6	33.9	31.6	2	1	8	17.7	17.3
1	10	1	25.1	26.7	-9	-1	2	22.4	22.0	-8	-1	3	13.9	13.0	2	-3	4	9.1	8.6	-1	0	6	12.5	14.5	2	-1	8	16.7	11.5
-5	12	1	24.9	19.9	0	-2	2	10.5	8.0	9	-1	3	22.3	19.2	3	-3	4	29.7	32.2	-5	10	6	18.0	21.5	-2	-1	8	15.5	14.8
8	-10	1	22.8	20.8	1	-2	2	19.5	16.8	-11	1	3	20.4	20.8	-3	-3	4	24.3	21.4	-9	9	6	14.6	13.3	-3	1	8	23.8	20.4
-4	5	1	12.8	18.3	-3	2	2	20.3	18.6	0	-2	3	28.3	27.5	-5	3	4	16.4	17.6	0	1	6	12.0	14.9	3	-1	8	25.6	29.5
-5	6	1	11.0	3.4	-3	-2	2	22.6	24.4	1	2	3	10.1	14.8	-7	3	4	20.2	22.1	-1	-1	6	22.2	26.1	-3	-1	8	19.4	28.2
-2	6	1	29.5	20.9	4	-2	2	12.9	15.9	-2	2	3	24.0	25.7	-10	3	4	17.1	23.2	1	-1	6	10.3	13.4					
-11	8	1	14.7	13.2	-4	-2	2	14.4	11.2	2	-2	3	36.8	39.1	2	4	4	20.1	17.9	-3	-1	6	18.5	20.3					
-2	1	1	10.4	10.7	-7	2	2	18.9	16.0	-3	-2	3	30.6	27.4	2	-4	4	23.6	25.2	-4	-1	6	15.1	20.9	-6	1	8	37.2	30.4
2	-1	1	18.1	15.9	0	-3	2	11.6	7.1	4	2	3	31.3	31.2	-3	4	4	23.1	18.6	5	1	6	24.7	24.8	-6	-1	8	14.2	16.6
-2	-1	1	8.6	4.6	1	3	2	33.0	33.1						-5	-4	4	17.9	15.5	5	-1	6	22.4	25.1	-8	-1	8	23.7	17.5
3	1	1	13.3	10.8	1	-3	2	18.8	14.0	-4	2	3	21.3	20.3	6	4	4	27.0	22.9	1	-2	6	34.8	34.9	1	2	8	15.0	14.5
3	-1	1	12.0	13.8	-3	3	2	14.5	5.3	-5	-2	3	21.5	20.5	-6	-4	4	27.6	33.4	-1	-2	6	17.6	18.1	-1	-2	8	34.5	33.3
-4	1	1	18.1	19.1	3	-3	2	22.1	10.9	-7	2	3	17.2	10.5	-6	4	4	38.1	33.4	3	2	6	21.2	29.9	2	2	8	43.9	41.7
-5	-1	1	13.4	14.5	-3	-3	2	25.8	29.4	0	3	3	33.6	35.4	-7	-4	4	27.6	19.3	-3	2	6	15.7	17.2	2	-2	8	26.3	28.1
-4	-1	1	24.4	22.5	-4	3	2	19.1	17.6	1	-3	3	22.2	18.0	-11	4	4	14.7	16.0	-3	-2	6	14.3	16.0	-2	2	8	22.7	19.4
7	1	1	16.0	17.2	-4	-3	2	13.2	6.7	2	3	3	13.7	16.7	-2	5	4	38.4	37.4	-4	-2	6	31.4	31.2	-5	2	8	23.7	30.9
-7	-1	1	22.1	11.9	-5	3	2	10.9	14.1	-2	-3	3	45.3	45.4	-2	-5	4	26.3	23.1	7	-2	6	18.1	16.0	-7	-2	8	17.3	23.8
-8	-1	1	15.4	23.6	5	-3	2	20.8	25.0	-3	3	3	44.0	39.4	-6	5	4	11.2	15.4	-8	2	6	35.1	41.0	-1	3	8	40.4	36.9
1	2	1	19.4	19.2	-7	-3	2	26.1	33.1	4	3	3	12.8	24.0	-7	5	4	15.2	24.4	1	3	6	14.7	12.1	-1	-3	8	15.2	14.3
-1	-2	1	17.4	8.4	-8	3	2	17.5	18.4	4	-3	3	14.5	19.9	-9	5	4	20.3	22.9	3	-3	6	14.3	23.3	2	3	8	27.0	23.2
2	3	1	23.4	24.4	8	-3	2	16.5	23.2	+4	+3	3	23.3	21.7	1	-6	4	14.2	12.3	-3	3	6	46.2	41.4	-2	-3	8	37.6	33.6
2	-3	1	13.1	4.2	-9	3	2	11.2	15.8	-6	3	3	14.0	19.1	-1	-6	4	47.3	43.2	-5	-3	6	15.2	17.8	+3	3	8	33.7	26.9
3	3	1	16.1	15.9	-1	4	2	45.1	38.6	-7	-3	3	19.7	25.1	-3	6	4	26.2	28.7	7	-3	6	15.8	15.8	3	-3	8	28.3	29.4
3	-3	1	12.9	15.0	1	-4	2	41.8	39.2	0	-4	3	20.7	15.7	-3	-6	4	21.4	19.8	-8	3	6	13.4	16.8	+5	3	8	24.8	26.1
-5	3	1	11.0	20.3	-1	-4	2	31.6	34.7	6	4	3	20.0	21.0	-5	6	4	31.7	32.3	-1	-4	6	15.6	17.2	+7	3	8	23.5	24.7
-8	-3	1	17.6	22.9	3	4	2	20.2	25.8	1	4	3	24.7	22.3	-5	-6	4	16.9	20.9	-3	4	6	43.8	38.8	-1	4	8	21.5	21.1
-1	-3	1	12.4	4.9	3	-4	2	13.5	8.7	+2	4	3	38.7	39.5	-7	6	4	12.4	16.8	4	-4	6	12.0	7.3	+2	4	8	23.9	21.2
2	4	1	26.0	31.9	-3	-4	2	11.1	11.4	-3	4	3	15.6	19.8	-7	7	4	32.6	32.9	-4	-4	6	19.2	23.1	2	-4	8	14.5	24.6
2	-4	1	12.6	12.0	4	-4	2	24.4	22.4	4	-4	3	12.4	15.0	-1	7	4	16.2	15.9	5	-4	6	20.9	27.7	-5	+4	8	27.7	20.4
-2	-4	1	27.6	22.8	-4	-4	2	25.2	19.1	+5	4	3	20.5	19.8	2	-7	4	17.0	21.2	-8	4	6	21.0	17.9	1	-5	8	15.8	15.6
3	5	1	13.0	10.5	7	-4	2	12.3	9.1	6	-4	3	16.2	22.1	7	-7	4	17.0	21.2	-8	5	6	20.0	17.8	-2	-5	8	19.8	28.2
-5	5	1	23.2	21.7	-7	-4	2	28.7	25.8	6	4	3	23.3	18.0	-1	-8	4	36.0	33.0	0	5	6	34.0	32.0	+5	5	8	24.0	17.3
7	-5	1	15.2	13.3	0	5	2	12.9	11.6	-6	-4	3	20.0	21.0	3	8	4	18.0	23.8	1	5	6	17.5	16.6	-5	-5	8	34.3	35.0
-10	6	1	23.7	28.4	0	-5	2	10.8	17.0	-7	4	3	20.5	19.5	-7	8	4	14.0	17.9	1	-5	6			-10	5	8	24.4	27.3
-1	6	1	23.5	18.8	-1	5	2	19.7	16.8	-8	4	3	12.5	7.5	-3	9	4	24.1	21.6						-3	6	8	29.4	21.9
-8	-4	1	28.7	24.6	-1	-5	2	20.4	14.6	-8	-4	3	19.2	9.0	-6	9	4	20.6	27.6	-1	-5	6	17.8	13.7	-8	6	8	28.2	24.0
+2	4	1	20.4	20.7	3	5	2	41.2	42.1	0	-5	3	15.4	21.0	7	-9	4	15.4	16.9	-4	5	6	21.3	21.9	3	-6	8	41.6	40.2
3	-4	1	12.8	10.2	-3	5	2	20.8	28.1	1	5	3	16.7	8.3	1	-10	4	20.1	16.0	-5	5	6	16.8	20.8	+6	6	8	29.0	32.4
-4	6	1	14.5	17.2	3	-5	2	14.6	6.4	2	5	3	13.0	11.4	-3	11	4	33.8	21.7	-8	-5	6	17.6	13.7	-2	7	8	23.8	27.8
4	-4	1	9.5	11.3	-3	-5	2	32.2	37.2	-2	-5	3	34.6	35.5	-5	11	4	26.9	24.6	3	-6	6	17.0	11.8	-5	7	8	15.4	11.4
-5	4	1	26.8	24.1	4	-5	2	13.6	12.7	-2	5	3	23.7	29.6	2	0	5	12.5	15.9	-5	6	6	14.5	15.7	-6	7	8	28.8	35.0
-5	-4	1	13.0	12.0	-5	5	2	11.1	13.8	2	-5	3	16.5	16.9	-4	0	5	19.0	23.4	5	-6	6	27.1	29.6	-3	8	8	24.8	28.4
6	4	1	24.8	27.5	7	5	2	15.8	22.2	-2	-5	3	18.6	17.3	6	0	5	18.2	12.3	1	-7	6	42.1	40.8	-5	8	8		
5	-4	1	14.3	14.8	7	-5	2	20.7	23.0	-3	5	3	20.5	24.3	-9	0	5	31.2	25.3	-1	-7	6	25.6	22.6					
-9	-4	1	18.7	20.8	-8	5	2	35.0	36.3	-4	5	3	30.2	30.3	0	1	5	21.9	22.6	-8	7	6	40.2	39.2					
0	5	1	15.4	26.6	8	-5	2	18.8	25.5	-7	5	3	14.6	16.3	2	-1	5	13.7	16.2	-4	8	6	25.1	28.4					
										-10	5	3	14.2	12.4	4	-1	5	23.0	28.8	-5	-8	6	19.9	16.6					

The two $[As_4S_{12}]$ clusters have nearly identical configurations. They are placed, however, in crystallographically distinct positions and are rotated slightly in opposite directions about [001]. As a result, each cluster of one kind shares sulfur atoms in common with three clusters of the other kind. This gives rise to two kinds of pyramidal attachments (Fig. 3). An $[AsS_3]$ pyramid may share two S atoms with two pyramids of an alternate cluster (the α-attachment); or alternatively, two pyramids of one cluster may share one sulfur atom each with a single pyramid of an alternate cluster (the β-attachment).

We define a Type I cluster of $[AsS_3]$ pyramids as one having two α-attachments (related by a rotation of 120°) and one β-attachment (Fig. 3). A Type II cluster has one α-attachment and two β-attachments (Fig. 3). Both Type I and Type II clusters are attached to three surrounding clusters of the opposite kind and their attachment configurations are enantiomorphous—whereas Type I has a $\beta\alpha\alpha$ configuration, the configuration of Type II may be denoted as $\beta'\beta'\alpha'$. The two kinds of clusters are interconnected, to give two-dimensional nets, two tetrahedra thick, stacked parallel to $(\bar{1}01)$ (Figs. 7, 8). The cubic point-group symmetry of an ideal individual cluster, $\bar{4}3m$, is reduced to triclinic, 1, when the attachments are built according to the steric requirements of the structure. In an untwinned state the whole net of interconnected clusters possesses the resulting triclinic symmetry. Adjacent nets are connected by Cu–S bonds and do not share common As and S atoms. The hexagon-shaped elongated mesh of the nets is filled by $[CuS_4]$ tetrahedra.

TABLE 2. Atomic Coordinates*

No.	Atom	x	y	z	No.	x	y	z
Me 1	As	.123**	.012**	.061**	S 1		vacant	
Me 2	As	.318	.180	.401	S 2	.332	.191	.681*
Me 3	As	.874	.014	.259	S 3	.833	.994*	.536**
Me 4	As	.156	.827	.348	S 4	.186	.777*	.603**
Me 5	As	.451	.594	.510	S 5		vacant	
Me 6	As	.663**	.789**	.868**	S 6	.653	.826	.104
Me 7	As	.233	.590	.714	S 7	.222	.597	.940
Me 8	As	.545	.432	.835	S 8	.539	.401	.096
Me 9	Cu	.962	.623	.943	S 9	.997	.584	.237
Me 10	Cu	.426	.788	.099	S 10	.426*	.797	.338**
Me 11	Cu	.569	.178	.146	S 11	.588	.165	.428
Me 12	Cu	.307	.415	.068	S 12	.260	.416	.342
Me 13	Cu	.838	.210	.960	S 13	.831	.184*	.174
Me 14	Cu	.915	.822	.614	S 14	.903	.824	.864**
Me 15	Cu	.356	.984	.749	S 15	.376	.969	.982*
Me 16	Cu	.069	.213	.665	S 16	.014	.169	.881
Me 17	Cu	.032	.375*	.347	S 17	.028	.385	.615
Me 18	Cu	.795*	.386*	.564*	S 18	.796*	.385*	.872*
Me 19	Cu	.598	.966	.494	S 19	.582	.959*	.719
Me 20	Cu	.720	.602	.185	S 20	.722	.595	.480

*Average standard errors of the fractional parameters for metal atoms are equal to 0.003, for sulfur atoms to 0.005. * denotes least accurate, strongly correlated values; ** denotes the values taken from the refinement with undetectable intensities included.*

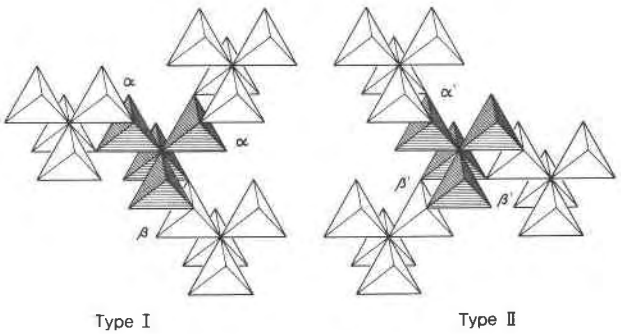

FIG. 3. $[As_4S_{12}]$ clusters of types I and II (both shaded). Sulfur atoms are situated at vertices of all clusters, with sulfur positions at center of clusters vacant. Arsenic atoms are situated near the centers of all tetrahedra (compare with Fig. 8).

The presence of the $[As_4S_{12}]$ clusters reveals kinship between the structures of sinnerite, $Cu_6As_4S_9$, and of nowackiite, $Cu_6Zn_3As_4S_{12}$ (Marumo, 1967). The latter is the only sulfosalt other than sinnerite in which the clusters have been observed. In nowackiite, however, clusters are not connected with each other, and they share all of their sulfur atoms with adjacent copper and zinc atoms only.

If we trace the network of the shortest As–S bonds within the above described layers $(\bar{1}01)$ of the $[As_4S_{12}]$ clusters, the layers decompose into a pattern of complicated, twisted, chain-like groups of conjugated $[AsS_3]$ pyramids. Two kinds of chains exist, with 3 and 5 conjugated pyramids respectively (Fig. 5), leading to compositions $[As_3S_7]$ and $[As_5S_{11}]$. Every S atom in the structure belongs to one of these groups, and is bound to one or two As atoms, so that the structural formula of sinnerite may be written $Cu_{12}[As_3S_7][As_5S_{11}]$. The structure of sinnerite (Figs. 6, 10) may be viewed as a close packing of the two groups, each kind being stacked in columns parallel to [001]. Each kind of group forms indistinct layers parallel to (010).

Both kinds of chains (Fig. 5) are built on the same patterns, except that the shorter $[As_3S_7]$ chain is a "half-finished" version of the complete $[As_5S_{11}]$ chain, the former lacking one of the two identical side-branches of the latter. The formation and shape of the chains are closely connected with the formation of the As_4 groups around the vacant sulfur sites. As the reader can trace in Figure 6, during growth of the chain an addition of a new $[AsS_3]$ pyramid to the chain leads either to completion of the envelope of an existing vacancy, or to the building of a new vacancy, thus perpetuating the $[As_4S_{12}]$ cluster motif. Half of each Type I cluster is created by an $[As_3S_7]$ group, while the other half contains portions of two $[As_5S_{11}]$

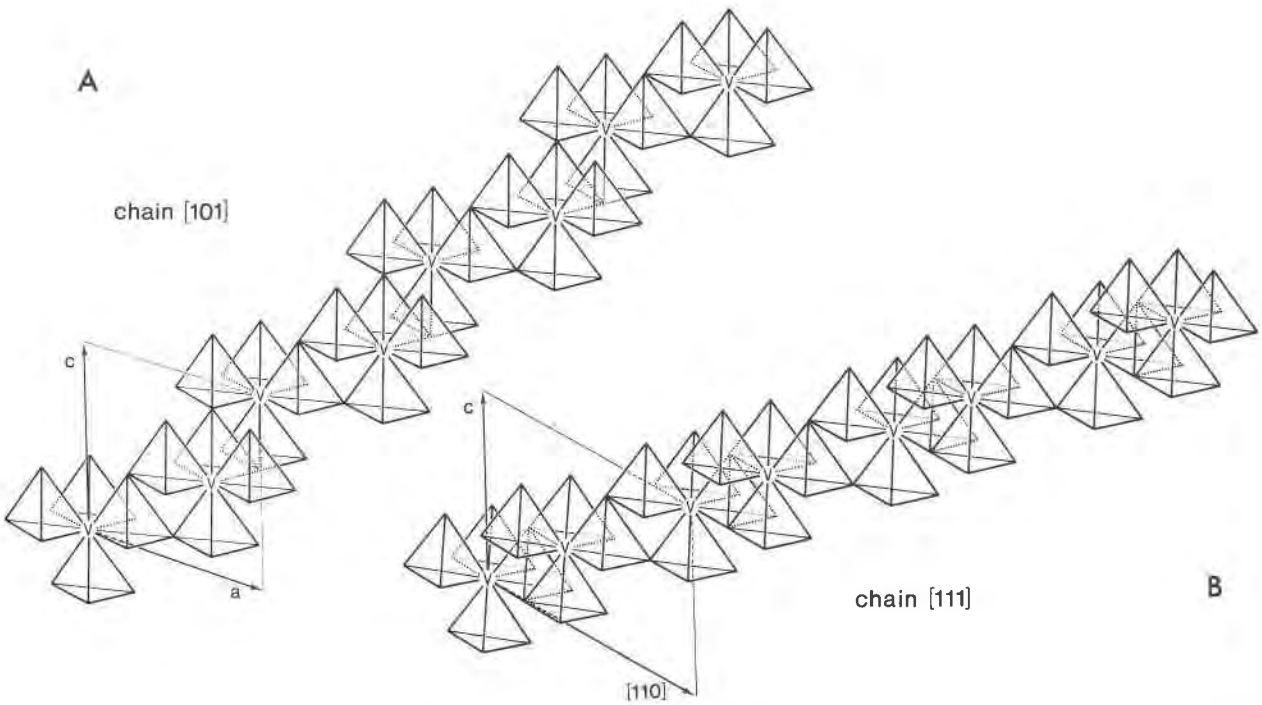

FIG. 4. Axonometric projection of chains of $[As_4S_{12}]$ clusters interconnected through common sulfur atoms. (A) chain parallel to [101]; (B) chain parallel to [111]. Sulfur vacancies denoted V.

chains. In the Type II cluster, 3/4 is accounted for by one $[As_5S_{11}]$ group, while the remaining 1/4 is part of an $[As_3S_7]$ group.

Three out of eight $[AsS_3]$ pyramids in the unit cell of sinnerite (As3, As7, As8) share one of their sulfur atoms (S6, S4, and S2, respectively) with another $[AsS_3]$ pyramid situated below them (Fig. 6) Due to the shortness of the As–S bond, the shared S atom is pulled out of the respective average atomic level and the $[AsS_3]$ pyramid in question is slightly rotated around its three-fold axis. Thus the S atoms 13, 17, and 18 become slightly displaced in the opposite direction, together with the corresponding Cu atoms bound to them by the vertical Cu–S bonds. The latter

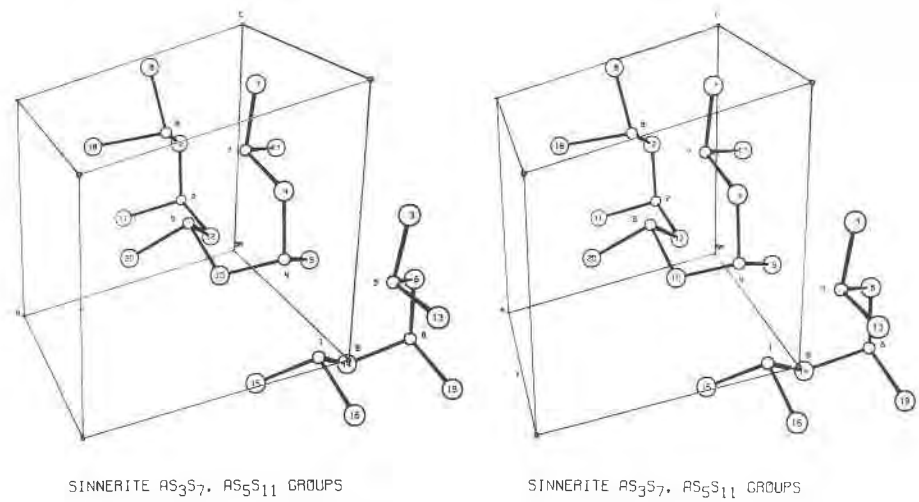

FIG. 5. Stereoscopic view of $[As_3S_7]$ and $[As_5S_{11}]$ groups from the crystal of sinnerite. Arsenic atoms (small spheres) are numbered the same as the sulfur atoms (large spheres) above them. Positions of some sulfur atoms are partly idealized. (Drawn by Dr. H. T. Evans, Jr., U. S. Geological Survey, using the ORTEP program of C. K. Johnson, Oak Ridge National Laboratories).

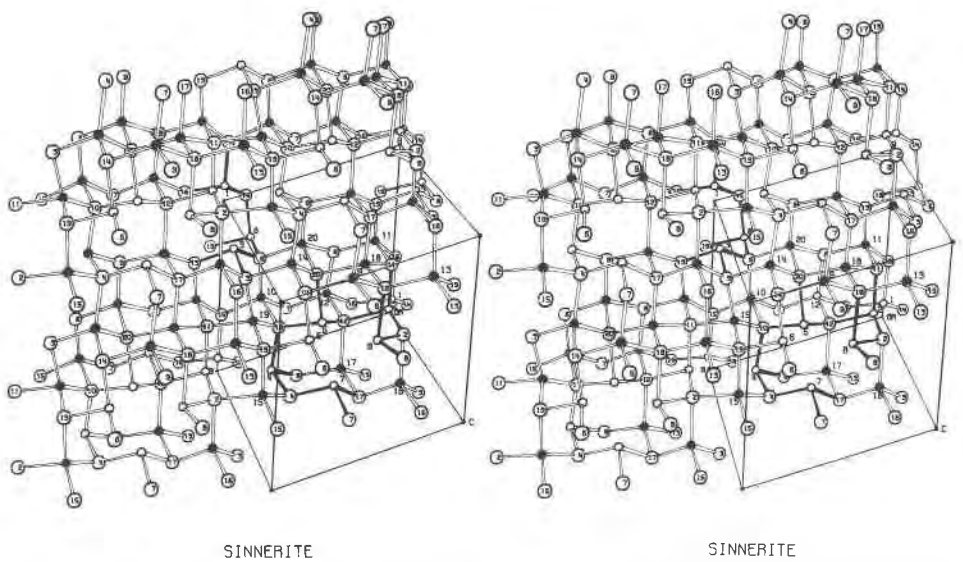

FIG. 6. Crystal structure of sinnerite. Stereoscopic view along the *c* axis. Arsenic atoms (small open spheres) and copper atoms (small filled spheres) are numbered the same as sulfur atoms immediately in front of them. Positions of some sulfur atoms are partly idealized. (Drawn by Dr. H. T. Evans, Jr., U. S. Geological Survey, using the ORTEP program of C. K. Johnson, Oak Ridge National Laboratories).

form the spiral arrangement parallel to [001] (Fig. 6) which is most prominent in the difference structure, being still unobscured by positional correlations of the full structure. At the same time Cu 13, 17, and 18 represent a center of the largest concentration of Cu tetrahedra in the structure (Cu 9, 11, 13, 16, 17, 18), bracketed by two $[As_3S_7]$ and two $[As_5S_{11}]$ groups (Fig. 6). The displacement of the Cu–S pairs—13, 17, and 18—thus represents also an adjustment of the $[CuS_4]$ tetrahedra to the shorter interatomic distances of the bracketing As–S chains. Unfortunately the low accuracy of the structure determination does not permit study of the details of the coordination of the displaced Cu atoms.

Twinning

The layer, parallel to $(\bar{1}01)$, of interconnected $[As_4S_{12}]$ clusters may be treated as consisting either of laterally interconnected zig-zag chains parallel to [101] or of similar chains parallel to [111]. The two types of chains (Figs. 4a and 4b) consist of alternating clusters of Types I and II but differ in the way adjacent clusters are interconnected. Both kinds, however, have their Type I and Type II clusters related by an internal *n*-glide plane. The glide plane is not valid for any of the chain attachments (side-branches).

When an $[As_4S_{12}]$ cluster fills a gap in an existing cluster-chain of one of the above described types, its position and the way of attachment to the existing clusters (always an $\alpha\beta$ or $\alpha'\beta'$ attachment) are fixed beforehand. But whenever a new cluster is being attached laterally on the exposed side of a complete chain (Fig. 4), or to a whole layer, $(1\bar{1}0)$ or (010) of such chains, two to four options are left for the attachment.

Only two positional options exist for the lateral clusters being attached to the [111] chains, exposed on the planes $(1\bar{1}0)$ or $(\bar{1}10)$. This process may be followed on Figure 7 moving from right to left. According to the option selected, the attachment may or may not be a mirror image of the cluster attachments on the other completed, and now unexposed, side of the chain. The latter case completes the exposed chain as an –I–II–I–II– asymmetric chain and causes the structure to propagate along its original translation vectors. The former, however, produces symmetrical chains composed of clusters of one type only, that is, –I–I′–I–I′– or –II–II′–II–II′ chains. As the cluster type of the lateral cluster is already predetermined by the way the cluster attaches itself to the original chain, the validity of the *n*-glide plane will be extended to the whole regular structure, growing after the symmetrical chain configuration has occurred. Thus, a twinning results with an *n*-glide plane $(1\bar{1}0)$ both as a twin plane and as a contact plane.

The situation on the (010) and $(0\bar{1}0)$ faces, which expose the [101] chains, is more complicated (Figs. 8, 9). Both the internal symmetry of each [101] chain and the way of their packing into the (010) slab are

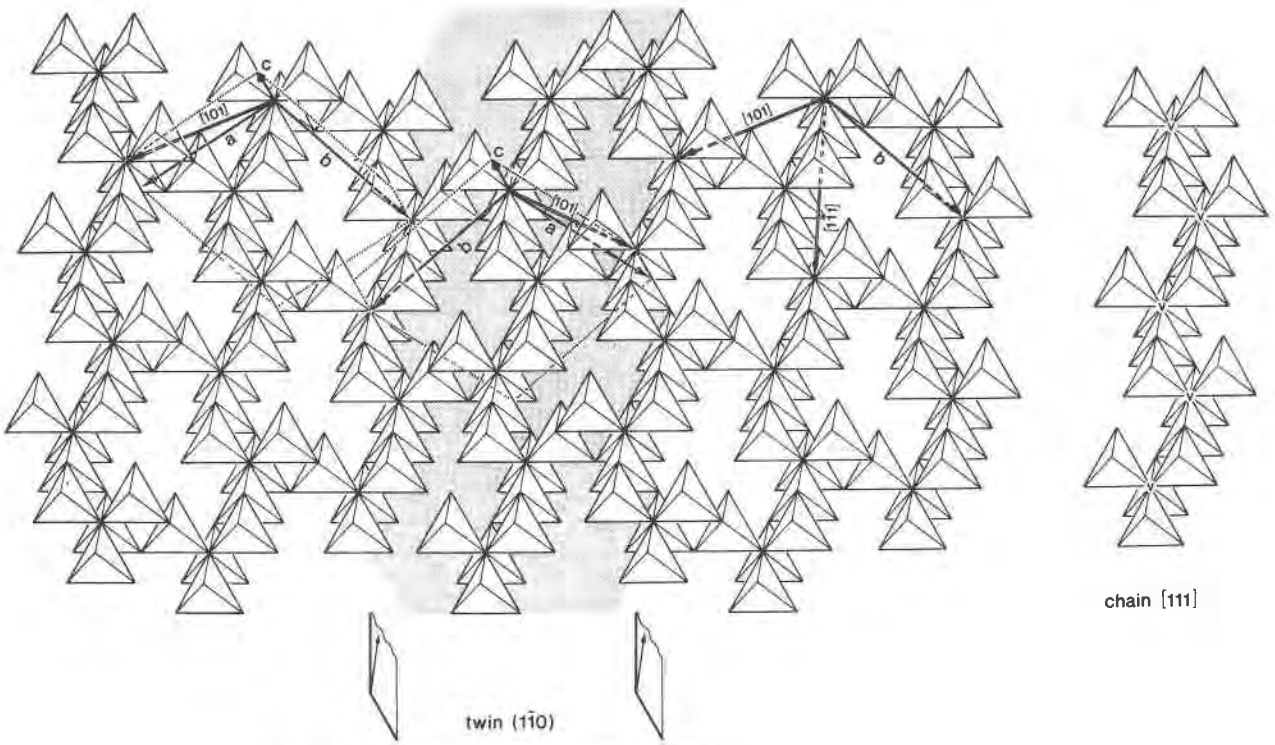

FIG. 7. Axonometric projection of one (10$\bar{1}$) layer of interconnected [As_4S_{12}] clusters with twin lamella (1$\bar{1}$0) shown shaded. The *n*-glide twin planes, (0$\bar{1}$0), are indicated in lower portion of the figure, the cluster chain [111] in the right-hand section.

orthorhombic. A single [101] chain, without lateral attachments, possesses a glide plane parallel to (010), with the glide component along the chain axis. Furthermore it displays a mirror plane indexed as ($\bar{4}$1$\bar{4}$) in the sinnerite unit cell parallel to the chain elongation and perpendicular to the glide plane. Their intersection in the chain axis represents a two-fold screw axis [101]. The packing preserves these symmetry elements and thus generates additional glide planes parallel to the ($\bar{4}$1$\bar{4}$) mirror planes and two-fold axes parallel to, and spaced half-way between the 2_1 axes. Consequently the (010) slab of the [101] chains can be described by an orthorhombic *C*-centered "cell" with the (primed)axes, related to the true-cell axes as follows: $a' = a + c$; $b' = c - a$; and c', which represents the slab thickness, given as $c' = d_{010}$. This means, that within each (010) slab of the cluster chains the *a* and *c* axes of sinnerite become crystallographically identical, related by the orthorhombic symmetry of the slab. In this case both the α- and β-type attachments may each be found in two mirror-related positions (Fig. 9). These four options result in one simple translation and three twinning laws, all with the same contact plane.

On the (010) contact plane, for example (Fig. 8), the β linkage of a lateral cluster on the exposed chain propagates the original structure along the $t_{0\bar{1}0}$ translation (Fig. 9). The mirror-related β''-linkage (Fig. 9) produces a twinning with the ($\bar{4}$1$\bar{4}$) mirror planes and the interspaced ($\bar{4}$1$\bar{4}$) glide planes, which are converted from the partial symmetry elements of the (010) slab into symmetry elements that define the twinning. The new *a* and *c* take the orientation of the original *c* and *a* axes, respectively. The α-linkage produces a twinning with an *n*-glide twin plane (010), and with the original *a* and *c* directions preserved in the twin (Figs. 8 and 9). The β- and α-linkages produce asymmetric and symmetric cluster-chains, respectively, as in the case of the (1$\bar{1}$0) contact plane. Finally, the α''-linkage (Fig. 9) produces a ($\bar{4}$1$\bar{4}$) mirror image of the (010) twin, so that the *a* and *c* directions are again interchanged. The system of 2 and 2_1 parallel to [101] defines the twin law in this case (Table 2).

With respect to the twinning on the contact planes (010) or (0$\bar{1}$0), sinnerite represents an OD structure composed of disordered mutually identical layers (010) with internal orthorhombic symmetry. Using the nomenclature of Dornberger-Schiff (1966) for OD groupoids, with the intra-layer identity vectors

a',b' and the layer thickness c' defined above, the "ebene Raumgruppe" of the layer is $C\ 2\ m$ (a'). The last symbol denotes the glide plane perpendicular to the slab thickness, with the glide component of $a'/2$. The layer (slab) in question has Miller indices (001)′ in this notation (Table 3).

The interlayer identity vector, in the (0$\bar{1}$0) contact plane, from the n^{th} to the $(n + 1)^{th}$ (0$\bar{1}$0) slab is, in the case of the β-linkage (= unit vector $-\mathbf{b}$), defined as $\mathbf{t} = \frac{1}{4}\mathbf{a}' - \frac{1}{8}\mathbf{b}' + \mathbf{c}'$. Due to the reciprocal relationship of the α- and β- linkages, the same identity vector for the α-linkage has the same length and an orientation $\mathbf{t} = -\frac{1}{4}\mathbf{a}' + \frac{1}{8}\mathbf{b}' + \mathbf{c}'$. The partial symmetry operations relating two adjacent slabs will then read as follows:

$$\{2_{\bar{\frac{1}{2}}} n_{2,\frac{1}{2}}(n_{\bar{\frac{1}{2}},\frac{1}{2}})\} \text{ for the } \beta\text{-linkage}$$

and

$$\{2_{\frac{1}{2}} n_{2,\bar{\frac{1}{2}}}(n_{\frac{1}{2},\frac{1}{2}})\} \text{ for the } \alpha\text{-linkage}$$

where, as a generalization of the concept used for the normal space-group notation, the subscripts have the value of the minimal translation components multiplied by two and are always arranged in the cyclic order of basic vectors **a**′, **b**′, **c**′, following after the vector normal to the plane in question (Dornberger-Schiff, 1966).

The third system of asymmetric zig-zagged chains, parallel to [010], cannot produce twinning phenomena corresponding to those on the two above described systems of internally symmetrical chains. Thus, both the twin plane (410) and the three-fold axis parallel to [001] were confirmed to be of derived (secondary) nature (Makovicky and Skinner, 1972).

The concept of the $[As_4S_{12}]$ clusters and of their chains has proved extremely useful in the complete analysis of twinning possibilities and gave an effective description of the sinnerite twinning in terms of geometry and symmetry. If individual $[As_3S_7]$ and $[As_5S_{11}]$ groups are considered instead, the geometrical conditions become very complicated. This approach, however, is elegant in a crystal chemical explanation of twinning and is intriguing in considering the mechanisms of crystal growth.

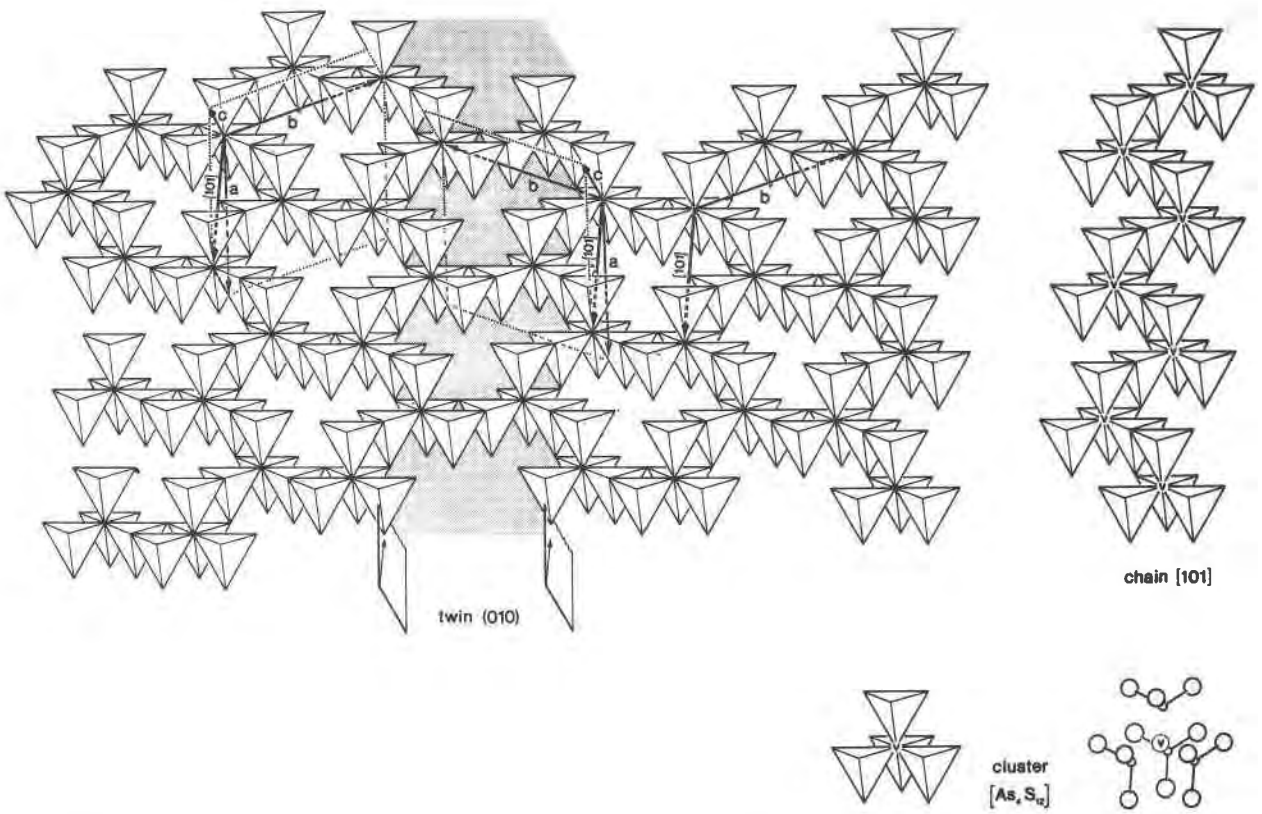

FIG. 8. Axonometric projection of one layer of interconnected clusters of $[As_4S_{12}]$ parallel to (10$\bar{1}$). Shaded area indicates the (010) twin lamella, with the positions of both n-glide twin planes below. The right-hand portion of the figure contains the cluster chain [101] and an individual $[As_4S_{12}]$ cluster in both schematic and structural representations. Sulfur vacancies denoted V.

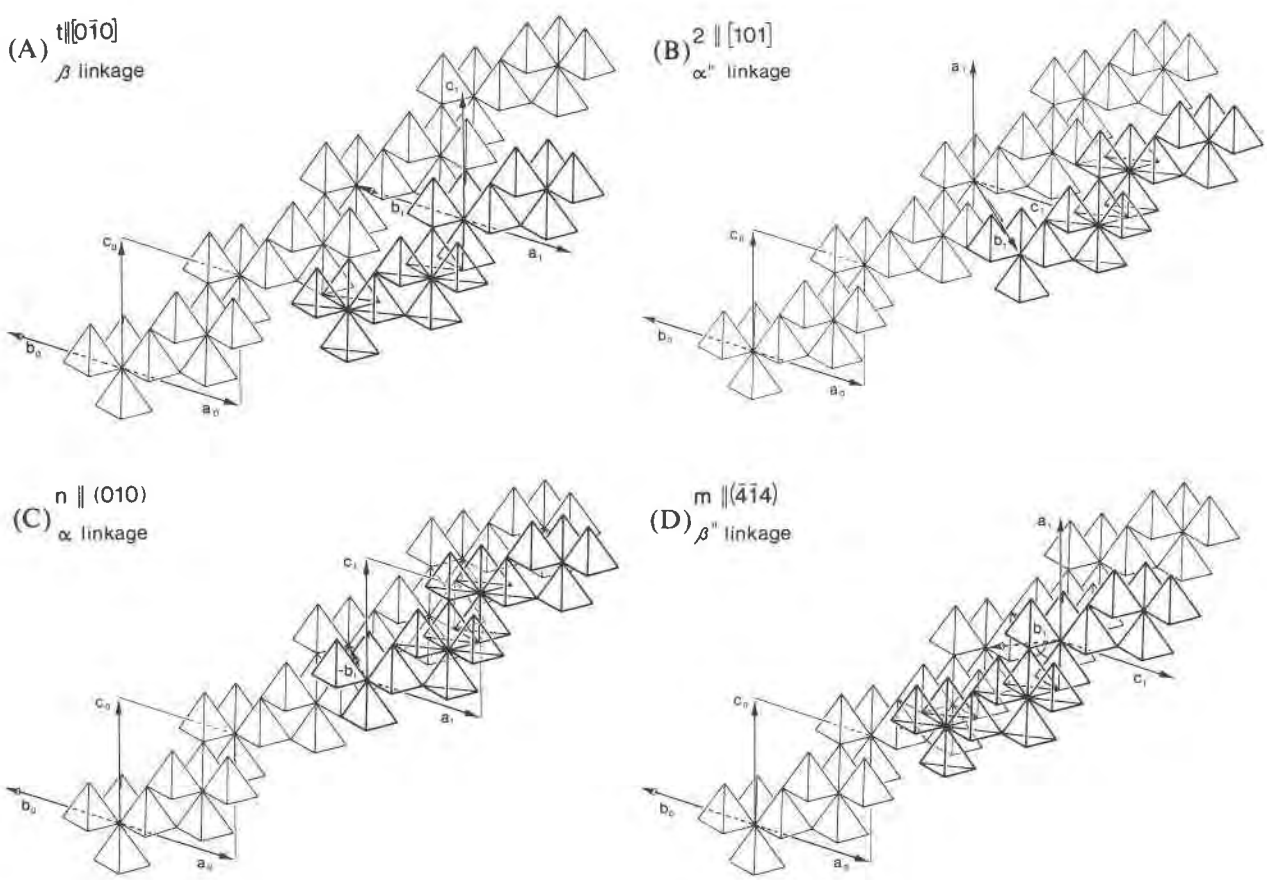

FIG. 9. OD phenomena on the (0$\bar{1}$0) growing face of sinnerite. The newly formed chain [101] of clusters (bold outlines, foreground) may assume four different positions with respect to the existing chain [101] (light outlines, background). Crystallographic axes in the original orientation have subscripts 0. Axes in the new orientation, resulting from mode of the chain apposition, have subscripts 1. Linkage modes and resulting twin elements are indicated. The apparent parallelism between a_0 and b_0 and between a_1 and b_1 is an illusion produced by the angle of projection.

As mentioned above, the $[As_3S_7]$ groups form indistinct layers parallel to (010), alternating with thicker layers of the $[As_5S_{11}]$ groups (Fig. 10). If the (0$\bar{1}$0) face is exposed, we may start the analysis with a complete layer of the $[As_3S_7]$ chains deposited (Fig. 11, empty circles) on the last layer of the $[As_5S_{11}]$ chains. The $[As_3S_7]$ layer displays the system of reflection and glide planes (4$\bar{1}$4), and mutually identical *a* and *c* directions. The next layer of As–S groups (Fig. 11, medium dark circles) may be composed of one of the following types:

(a) $[As_5S_{11}]$ groups are symmetrically nested upon the previous layer by means of one of their $[As_3S_7]'$-mimicking side-branches. They extend asymmetrically with the other side-branch either oriented identical to the $[As_5S_{11}]$ layer below it (Fig. 11, left, $t_{0\bar{1}0}$ case) or oriented by twin law $m \parallel (4\bar{1}4)$ (Fig. 11, upper right).

(b) $[As_3S_7]'$ groups instead of the complete $[As_5S_{11}]$ groups (lower part of Fig. 11). The symmetry planes of the $[As_3S_7]$ layer remain preserved also in the $[As_3S_7]'$ layer. After this an $[As_5S_{11}]$ layer must follow (the darkest circles). These $[As_5S_{11}]$ groups will be the (010)-mirror images of either the normal $[As_5S_{11}]$ groups (twin law: $n \parallel (010)$, lower center of Fig. 11), or of the reversed ones (twin law: $2 \parallel [101]$, lower right-hand corner of Fig. 11). Columns of the $[As_3S_7]$ and $[As_5S_{11}]$ groups will always follow the new *c*-axis orientation of the twin.

Twinning on ($\bar{1}$10) involves, similarly, the formation of a pure $[As_3S_7]$ and $[As_3S_7]'$ layer in ($\bar{1}$10), instead of a combined $[As_3S_7]$ and $[As_5S_{11}]$ one (Fig. 10). The stacking of the two kinds of As–S groups after this layer is *n*-glide related to the original sequence. Due to the asymmetry of the structure the

TABLE 3. Summary of Twin Elements, OD Phenomena, and Structural Description of Primary Twin Laws in Sinnerite*

twin law	contact plane	twin law in subcell notation	contact plane in subcell notation	type of the lateral cluster attachment to the [101] chain	relationships between axes of original (0) and twinned (1) individuals	symmetry and interlayer vectors of the OD (boundary) layer (crystallogr. elements of the layer are primed)
$\vec{t}_{0\bar{1}0}$	$(0\bar{1}0)$	-	$(1\bar{1}0)$	β	$a_1 = a_0$ $c_1 = c_0$	layer $(0\bar{1}0) \equiv (001)'$ with $\vec{a}' = \vec{a} + \vec{c}$ $\vec{b}' = \vec{c} - \vec{a}$ $\vec{c}' = \vec{d}_{0\bar{1}0}$ orthorhombic C 2 m (a′)
$m\|\|(\bar{4}\bar{1}4)$	$(0\bar{1}0)$	$m\|\|(110)$	$(1\bar{1}0)$	β''	$a_1 = c_0$ $c_1 = a_0$	
$n\|\|(010)$	$(0\bar{1}0)$	$n\|\|(1\bar{1}0)$	$(1\bar{1}0)$	α	$a_1 = a_0$ $c_1 = c_0$	
$2\|\|[101]$	$(0\bar{1}0)$	$2\|\|[001]$	$(1\bar{1}0)$	α''	$a_1 = c_0$ $c_1 = a_0$	

twin law	contact plane	twin law in subcell notation	contact plane in subcell notation	type of the lateral cluster attachment to the [111] chain	relationships between axes of original (0) and twinned (1) individuals	symmetry and interlayer vectors of the OD (boundary) layer (crystallogr. elements of the layer are primed)
$\vec{t}_{1\bar{1}0}$	$(1\bar{1}0)$	-	$(10\bar{1})$	α	$c_1 = c_0$ $[110]_1 = [110]_0$	layer $(1\bar{1}0) \equiv (010)'$ with $\vec{a}' = [\overrightarrow{1\bar{1}0}]$ $\vec{b}' = \frac{1}{2}\vec{d}_{1\bar{1}0}$ $\vec{c}' = \vec{c}$ monoclinic P 1 (n) 1
$n\|\|(1\bar{1}0)$	$(1\bar{1}0)$	$n\|\|(10\bar{1})$	$(10\bar{1})$	β	$c_1 = c_0$ $[110]_1 = [110]_0$	

twin law	interlayer identity vector of the OD (boundary) layer (crystallogr. elements of the layer are primed)	sequence of consecutive $[A_iS_j]$ layers $(0\bar{1}0)$ (twinned part of the structure is underlined; Note: underlined letter indicates a symmetry operator and [x] denotes the vector [x, y, z] for all atoms, one after another, of a given group A_iS_j.
$\vec{t}_{0\bar{1}0}$	$\vec{t} = \frac{1}{4}\vec{a}' - \frac{1}{8}\vec{b}' + \vec{c}'$	$\longrightarrow[As_5S_{11}] \longrightarrow [As_3S_7] \longrightarrow [As_5S_{11}] \longrightarrow [As_3S_7] \longrightarrow [As_5S_{11}] \longrightarrow$
m $(\bar{4}\bar{1}4)$	$\vec{t} = \frac{1}{4}\vec{a}' + \frac{1}{8}\vec{b}' + \vec{c}'$	$\longrightarrow[As_5S_{11}] \longrightarrow [As_3S_7] \longrightarrow \underline{[As_5S_{11}]' \longrightarrow [As_3S_7]' \longrightarrow [As_5S_{11}]' \longrightarrow}$ where $[x]' = \underline{m}_{\bar{4}\bar{1}4} \cdot [x]^T$ and $\underline{[As_3S_7]' \equiv [As_3S_7]}$ translated
n (010)	$\vec{t} = -\frac{1}{4}\vec{a}' + \frac{1}{8}\vec{b}' + \vec{c}'$	$\longrightarrow[As_5S_{11}] \longrightarrow [As_3S_7] \longrightarrow \underline{[As_3S_7]' \longrightarrow [As_5S_{11}]' \longrightarrow [As_3S_7]' \longrightarrow}$ where $[x]' = \underline{n}_{010} \cdot [x]^T$ so that $\underline{[As_3S_7]' \not\equiv [As_3S_7]}$ translated
2 [101]	$\vec{t} = -\frac{1}{4}\vec{a}' - \frac{1}{8}\vec{b}' + \vec{c}'$	$\longrightarrow[As_5S_{11}] \longrightarrow [As_3S_7] \longrightarrow \underline{[As_3S_7]' \longrightarrow [As_5S_{11}]' \longrightarrow [As_3S_7]' \longrightarrow}$ where $[x]' = \underline{2}_{[101]} \cdot [x]^T$ so that $\underline{[As_3S_7]' \not\equiv [As_3S_7]}$ translated
	interlayer identity vector of the OD (boundary) layer (crystallogr. elements of the layer are primed)	sequence of consecutive $[A_iS_j]$ layers $(1\bar{1}0)$ (twinned part of the structure is underlined; combination of different groups in one growth layer is indicated by the sign of &)
$\vec{t}_{1\bar{1}0}$	$\vec{t} = \frac{2}{5}\vec{a}' + \vec{b}' - \frac{1}{5}\vec{c}'$	$\longrightarrow[As_3S_7] \,\&\, [As_5S_{11}] \longrightarrow [As_3S_7] \,\&\, [As_5S_{11}] \longrightarrow [As_3S_7] \,\&\, [As_5S_{11}] \longrightarrow$
n $(1\bar{1}0)$	$\vec{t} = -\frac{2}{5}\vec{a}' + \vec{b}' + \frac{1}{5}\vec{c}'$	$\longrightarrow[As_3S_7] \,\&\, [As_5S_{11}] \longrightarrow \underline{[As_5S_{11}] \,\&\, [As_5S_{11}]' \longrightarrow [As_3S_7]' \,\&\, [As_5S_{11}]' \longrightarrow}$ where $[x]' = \underline{n}_{1\bar{1}0} \cdot [x]^T$

* Crystallographic elements of the sinnerite lattice are unprimed; elements given in terms of the internal periodicity of the boundary layers (7th and 8th columns) are primed. Subcell notation relates only to the 3rd and 4th columns. In the last column, the $[A_iS_j]$ groups of the original individual are umprimed; those transformed by twin operations are primed. Explanation of the α and β type linkages is given in the text.

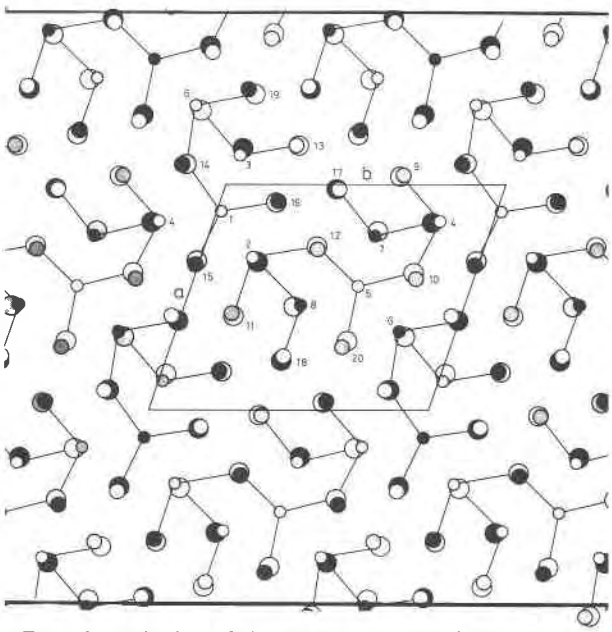

FIG. 10. Projection of the crystal structure of sinnerite along [001] showing the ordering scheme of the $[As_3S_7]$ and $[As_5S_{11}]$ groups in an untwinned crystal. Only the short arsenic–sulfur bonds are indicated. Circles in order of increasing sizes are arsenic, copper, and sulfur. Shading indicates the three structural layers, A, B, C formed by metal and sulfur atoms with close z coordinates. Metal and sulfur atoms with nearly identical x and y coordinates are numbered identically. Positions of sulfur atoms are partly idealized to conform with interatomic distances from well refined structures.

processes on the (010) and (1$\bar{1}$0) faces are reversed to those on (0$\bar{1}$0) and ($\bar{1}$10), thus involving double layers of the $[As_5S_{11}]$ and $[As_5S_{11}]'$ groups instead of those of the $[As_3S_7]$ and $[As_3S_7]'$ groups.

In spite of the variations in sequences of the $[As_3S_7]$ and $[As_5S_{11}]$ groups during twinning, none of the twin laws changes the sequences of chemical compositions of the mono-atomic structural layers on the crystal faces (010) or (1$\bar{1}$0) from those observed during the normal growth. In all cases twinning, as for the distribution of As and Cu atoms over the metal sites, amounts to a shift of the whole mono-atomic structural layer by one of the two shortest metal–metal vectors situated in the plane of the layer. The total chemical composition of the layer and the distribution pattern of metal atoms in it remain preserved. Thus, the twinning in sinnerite is not hindered by any compositional barriers.

Sinnerite may be regarded as an OD structure composed of two types of acentric, finite 3-dimensional building elements with several possible mutual orientations (coupling modes) and resulting spatial relationships. The OD, and related twinning processes, however, can take place only when crystal forms (010) and (1$\bar{1}$0) are developed as the growing crystal faces. This is not a frequent case, *e.g.*, the synthetic sinnerite exhibits growth mainly on (001) and (100), and the frequency of twinning is considerably lower than theoretically possible.

Consecutive application of any non-polysynthetic sequence of the described primary twin laws (Table 3 and 4) only occasionally leads to a twin operation between the last and some of the previous As_5S_{11} or As_3S_7 individuals. The last individual, however, will always be related to all the previous ones by definite symmetry operations, representing symmetry operations of the cubic space group $F\bar{4}3m$ describing the sphalerite-like substructure. Consequently, sinnerite is twinned by reticular pseudomerohedry and all the primary as well as derived (secondary) twin laws restore almost ideally the pseudocubic sublattice. Only the primary laws also restore parts of the triclinic lattice, other than the sublattice points, and only they represent true laws explainable by the OD processes in the sinnerite structure. These two categories of twin laws are important to distinguish in very complex aggregates of intertwinned sinnerite individuals.

Alternate application of the twin laws (010) and (1$\bar{1}$0), to the very last individual obtained from the twinning processes, leads to a six-membered composite aggregate (Table 4 and Fig. 12). The c axes of all six individuals are in common and parallel to one of the three-fold axes of the cubic sublattice. Its total symmetry is $3m$. Twinning on the (010) contact plane, always common to two individuals of the six-

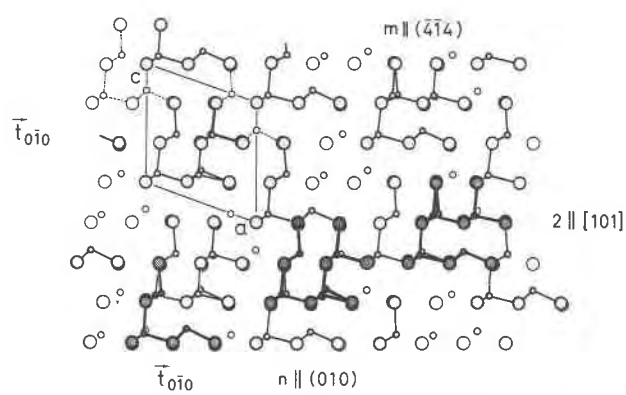

FIG. 11. Three different apposition levels of the As–S groups on (0$\bar{1}$0) indicated by shading and outlines. Bonding within the lowermost $[As_3S_7]$ groups (empty circles) is omitted except in the upper left-hand corner. The four different OD possibilities are indicated by the position of an individual $[As_5S_{11}]$ group of each case. A continuous $[As_3S_7]$ layer is built in the lower right-hand corner.

TABLE 4. Primary (underlined) and Derived Twin Operations for 12 out of 24 Individual Lattice Orientations of a Sinnerite Twin*

to twin individual number \ from twin individual number	1	2	3	4	5	6	1'	2'	3'	4'	5'	6'
1	1	$A\underline{m}(10\bar{1})$	$3^{-1}[111]$	$m(01\bar{1})$	$3[111]$	$B\underline{m}(1\bar{1}0)$	$C\underline{m}(110)$	$3^{-1}[1\bar{1}1]$	$\bar{4}[100]$	$3[\bar{1}11]$	$\bar{4}^{-1}[010]$	$D\underline{2}[001]$
2	$A\underline{m}(10\bar{1})$	1	$B\underline{m}(01\bar{1})$	$3^{-1}[111]$	$m(1\bar{1}0)$	$3[111]$	$3^{-1}[1\bar{1}1]$	$m(110)$	$3[\bar{1}11]$	$\bar{4}[100]$	$2[001]$	$\bar{4}^{-1}[010]$
3	$3[111]$	$B\underline{m}(01\bar{1})$	1	$A\underline{m}(1\bar{1}0)$	$3^{-1}[111]$	$m(10\bar{1})$	$\bar{4}^{-1}[010]$	$3[\bar{1}11]$	$m(110)$	$2[001]$	$\bar{4}[100]$	$3^{-1}[1\bar{1}1]$
4	$m(01\bar{1})$	$3[111]$	$A\underline{m}(1\bar{1}0)$	1	$B\underline{m}(10\bar{1})$	$3^{-1}[111]$	$3[\bar{1}11]$	$\bar{4}^{-1}[010]$	$2[001]$	$m(110)$	$3^{-1}[1\bar{1}1]$	$\bar{4}[100]$
5	$3^{-1}[111]$	$m(1\bar{1}0)$	$3[111]$	$B\underline{m}(10\bar{1})$	1	$A\underline{m}(01\bar{1})$	$\bar{4}[100]$	$2[001]$	$\bar{4}^{-1}[010]$	$3^{-1}[1\bar{1}1]$	$m(110)$	$3[\bar{1}11]$
6	$B\underline{m}(1\bar{1}0)$	$3^{-1}[111]$	$m(10\bar{1})$	$3[111]$	$A\underline{m}(01\bar{1})$	1	$D\underline{2}[001]$	$\bar{4}[100]$	$3^{-1}[1\bar{1}1]$	$\bar{4}^{-1}[010]$	$3[\bar{1}11]$	$C\underline{m}(110)$
1'	$C\underline{m}(110)$	$3[\bar{1}11]$	$\bar{4}[010]$	$3^{-1}[\bar{1}11]$	$\bar{4}^{-1}[100]$	$D\underline{2}[001]$	1	$A\underline{m}(011)$	$3[\bar{1}\bar{1}1]$	$m(101)$	$3^{-1}[\bar{1}\bar{1}1]$	$B\underline{m}(1\bar{1}0)$
2'	$3[\bar{1}11]$	$m(110)$	$3^{-1}[\bar{1}11]$	$\bar{4}[010]$	$2[001]$	$\bar{4}^{-1}[100]$	$A\underline{m}(011)$	1	$B\underline{m}(101)$	$3[\bar{1}\bar{1}1]$	$m(1\bar{1}0)$	$3^{-1}[\bar{1}\bar{1}1]$
3'	$\bar{4}^{-1}[100]$	$3^{-1}[\bar{1}11]$	$m(110)$	$2[001]$	$\bar{4}[010]$	$3[\bar{1}11]$	$3^{-1}[\bar{1}\bar{1}1]$	$B\underline{m}(101)$	1	$A\underline{m}(1\bar{1}0)$	$3[\bar{1}\bar{1}1]$	$m(011)$
4'	$3^{-1}[\bar{1}11]$	$\bar{4}^{-1}[100]$	$2[001]$	$m(110)$	$3[\bar{1}11]$	$\bar{4}[010]$	$m(101)$	$3^{-1}[\bar{1}\bar{1}1]$	$A\underline{m}(1\bar{1}0)$	1	$B\underline{m}(011)$	$3[\bar{1}\bar{1}1]$
5'	$\bar{4}[010]$	$2[001]$	$\bar{4}^{-1}[100]$	$3[\bar{1}11]$	$m(110)$	$3^{-1}[\bar{1}11]$	$3[\bar{1}\bar{1}1]$	$m(1\bar{1}0)$	$3^{-1}[\bar{1}\bar{1}1]$	$B\underline{m}(011)$	1	$A\underline{m}(101)$
6'	$D\underline{2}[001]$	$\bar{4}[010]$	$3[\bar{1}11]$	$\bar{4}^{-1}[100]$	$3^{-1}[\bar{1}11]$	$C\underline{m}(110)$	$B\underline{m}(1\bar{1}0)$	$3[\bar{1}\bar{1}1]$	$m(011)$	$3^{-1}[\bar{1}\bar{1}1]$	$A\underline{m}(101)$	1

* Twin operations are given in terms of the *pseudocubic sublattice* of the individual No. 1. Superscripts denote the following primary twin laws *in terms of the sinnerite unit cell:* A = twin law $n\|(1\bar{1}0)$; B = twin law $n\|(010)$; C = twin law $m\|(\bar{4}14)$; D = twin law $2\|[101]$. The relationships within and between the two above described six-member groups of twin individuals are representative of all relationships in the complete twin aggregate.

membered ring, may generate a new lattice orientation, related to one of the individuals by $(\bar{4}14)$ and to the opposite one by $2_{[101]}$ (Table 4). The new lattice will have the *c* axis parallel to another cubic threefold axis and will serve as a potential base of another 6-membered cluster of sinnerite individuals (Table 4 and Fig. 12). There are three contact planes of the (010) type in each of four possible six-membered rings and, through the twin laws $(\bar{4}14)$ and $2_{[101]}$ they serve as connecting points between the rings. In total, there are 36 true-twinning contacts, out of 276 distinct individual-to-individual symmetry relationships, present in a full 24-membered twin aggregate of sinnerite, giving the total symmetry of $\bar{4}3m$. All the primary twin operations belong to the *m* and *2* categories, the 3-fold and $4^{\pm 1}$ operations in all cases represent secondary laws only. Any cubic mirror plane will coincide consecutively with all three types of the primary twin planes, if appropriate pairs of lattice orientations are examined. Furthermore, it will interconnect a number of other pairs of lattice orientations as a secondary twin law.

The description of sinnerite twin laws in terms of the (pseudo) cubic sublattice, although efficient when the simplicity of indexing is of prime importance, does not distinguish in its pure form between the primary and secondary twin laws and gives no ex-

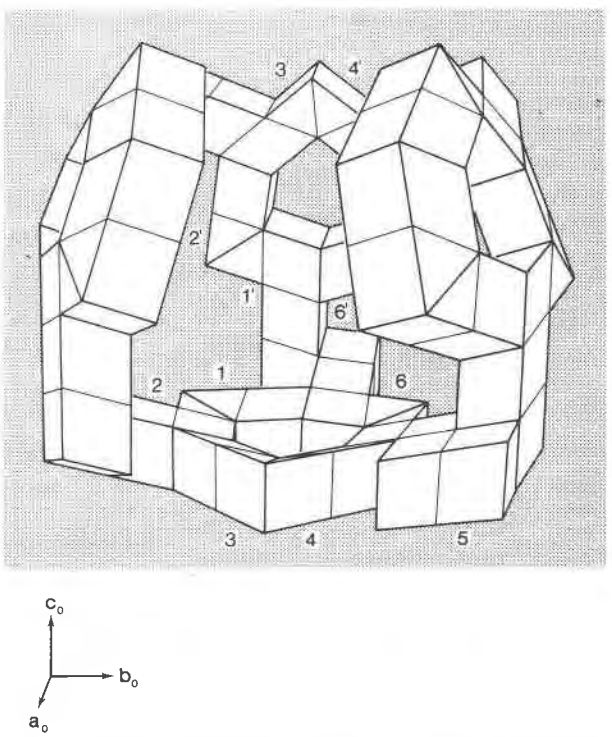

FIG. 12. Perspective drawing of an openwork model of a complete twin of sinnerite. Twin individuals are defined by means of their unit cells. Two out of four six-member rings are numbered in accordance with Table 4. The orientation of individual number 1 is indicated below the figure.

planations of the true nature of the twinning processes. The same holds concerning the attempts to describe the crystal structure of sinnerite in subcell notation. The cluster–cluster vectors expressed in terms of the cubic subcell acquire the following forms: $[\bar{1}\bar{1}1]$, $[\frac{3}{2}\bar{1}\frac{1}{2}]$ and [111] for the **a**, **b**, and **c** unit cell vectors, connecting clusters of the same type and $[\frac{1}{2}\frac{1}{2}1]$, or alternatively $[\frac{\bar{1}}{2}\frac{3}{2}0]$, for the [0.67, 0.42, 0.55] vectors, connecting clusters of opposite kind. The derivation of twinned positions using the above subcell notation fails, for example, to take into account the *n*-glide nature of some twin laws and gives no indication of the structural compatibility (*i.e.*, primary twin character) of various lattice orientations.

The two descriptions of sinnerite, in terms of the $[As_4S_{12}]$ clusters and in terms of the $[As_3S_7]$ and $[As_5S_{11}]$ groups, embrace the two basic crystal-chemical concepts which cooperated in building of a sinnerite crystal. Although the latter grew by the apposition or by an on-the-spot accretion of the shorter and longer As–S groups, the shape and packing of these groups are in direct connection with the distribution of the sulfur vacancies, with maintenance of local valency balance and with an overriding tetrahedral coordination in the structure.

The crystal structure of sinnerite is a typical example of a sulfosalt structure with a relatively low ratio of semimetal to metal (Makovicky, 1967). Consequently, the overall structure motif is determined mainly by the coordination properties of the latter species. Arsenic easily forms sulfosalt structures of this category with tetrahedrally coordinated copper because of convenient As^{III}–S bond lengths and S–As^{III}–S bond angles and because of the weak tendency of As^{III} to form higher-coordinated $p^3d^2s^2$ bonds instead of p^3 pyramids. Antimony does not form a corresponding structure of its own, nor does it substitute appreciably for arsenic in sinnerite —the maximum substitution is about 4.6 percent (Skinner and Luce, unpublished data).

Acknowledgments

The authors are indebted to Drs. Joan R. Clark, D. E. Appleman, H. T. Evans, Jr., and M. Ross of the U. S. Geological Survey, Washington, D. C., for their assistance with the intensity measurements and to H. T. Evans, Jr., for preparation of Figures 5 and 6. The assistance of Mrs. M. Makovicky, Mr. F. D. Luce, and Mrs. P. Kerley of Yale University, of Mrs. R. Larson, University of Copenhagen, and the stimulating points raised by Professor J. D. H. Donnay, Université de Montréal, Dr. H. T. Evans, Jr., and Professor F. Liebau, Universitat Kiel, are gratefully acknowledged. This work was supported by NSF grant GA-4142.

References

AHMED, R. R. (1968) NRC-8, Fourier for distorted and undistorted nets. Division of Pure Physics, Nat. Research Council of Canada, Ottawa, Canada.

BRADLEY, A. J. (1924) The crystal structure of metallic arsenic. *Phil. Mag., 6th Ser.* **47,** 657–671.

BUSING, W. R., K. O. MARTIN, AND H. A. LEVY (1962) ORFLS, a Fortran crystallographic least-squares program. U.S. Nat. Tech. Inform. Laboratory, Tennessee.

CROMER, D. T. (1965) Anomalous dispersion corrections computed from self-consistent field relativistic Dirac-Slater wave functions. *Acta Crystallogr.* **18,** 17–23.

———, AND J. T. WABER (1965) Scattering factors computed from relativistic Dirac-Slater wave functions. *Acta Crystallogr.* **18,** 104–109.

DORNBERGER-SCHIFF, K. (1966) *Lehrgan über OD-Strukturen.* Akademie-Verlag, Berlin, 135 p.

MAKOVICKY, E. (1967) Bemerkungen zu der Systematik und Mineralogie der Sulfosalze der Metalle der 5. *Gruppe. Geol. Sbnornik (Bratislava),* **18,** 39–64.

———, AND B. J. SKINNER (1972) Studies of the sulfosalts of copper, II. The crystallography and composition of sinnerite, $Cu_6As_4S_9$. *Am. Mineral.* **57,** 824–834.

MARUMO, F. (1967) The crystal structure of nowackiite, $Cu_6Zn_3As_4S_{12}$. *Z. Kristallogr.* **124,** 352–368.

———, AND W. NOWACKI (1964) The crystal structure of lautite and of sinnerite, a new mineral from the Lengenbach Quarry. *Schweiz. Mineral. Petrogr. Mitt.* **44,** 439–454.

MASKE, S., AND B. J. SKINNER (1971) Studies of the sulfosalts of copper, I. Phases and phase relations in the system Cu-As-S. *Econ. Geol.* **66,** 901–918.

TAKEUCHI, Y., AND R. SADANAGA (1969) Structural principles and classification of sulfosalts. *Z. Kristallogr.* **130,** 346–368.

WUENSCH, J. B., AND C. T. PREWITT (1965) Corrections for X-ray absorption by a crystal of arbitrary shape. *Z. Kristallogr.* **122,** 24–59.

———, Y. TAKEUCHI, AND W. NOWACKI (1966) Refinement of the crystal structure of binnite, $Cu_{12}As_4S_{13}$. *Z. Kristallogr.* **135,** 93–119.

Manuscript received, October 5, 1973; accepted for publication, July 2, 1975.